Journal of Magnetic Resonance **149,** 196–203 (2001)
doi:10.1006/jmre.2001.2298, available online at http://www.idealibrary.com on IDEAL®

A Q-Band Pulse EPR/ENDOR Spectrometer and the Implementation of Advanced One- and Two-Dimensional Pulse EPR Methodology

I. Gromov,*,[1] J. Shane,* J. Forrer,* R. Rakhmatoullin,† Yu. Rozentzwaig,† and A. Schweiger*

*Laboratory of Physical Chemistry, ETH-Zentrum, Swiss Federal Institute of Technology, CH-8092 Zürich, Switzerland; and †Laboratory of Magnetic Radiospectroscopy and Quantum Electronics, Kazan State University, 420008 Tatarstan, Russian Federation

Received September 18, 2000; revised January 23, 2001; published online March 20, 2001

A versatile high-power pulse Q-band EPR spectrometer operating at 34.5–35.5 GHz and in a temperature range of 4–300 K is described. The spectrometer allows one to perform one- and two-dimensional multifrequency pulse EPR and pulse ENDOR experiments, as well as continuous wave experiments. It is equipped with two microwave sources and four microwave channels to generate pulse sequences with different amplitudes, phases, and carrier frequencies. A microwave pulse power of up to 100 W is available. Two channels form radiofrequency pulses with adjustable phases for ENDOR experiments. The spectrometer performance is demonstrated by single crystal pulse ENDOR experiments on a copper complex. A HYSCORE experiment demonstrates that the advantages of high-field EPR and correlation spectroscopy can be combined and exploited at Q-band. Furthermore, we illustrate how this combination can be used in cases where the HYSCORE experiment is no longer effective at 35 GHz because of the shallow modulation depth. Even in cases where the echo modulation is virtually absent in the HYSCORE experiment at Q-band, matched microwave pulses allow one to get HYSCORE spectra with a signal-to-noise ratio as good as at X-band. Finally, it is shown that the high microwave power, the short pulses, and the broad resonator bandwidth make the spectrometer well suited to Fourier transform EPR experiments. © 2001 Academic Press

Key Words: **ESEEM; HYSCORE; matching; FT EPR.**

INTRODUCTION

Pulse electron paramagnetic resonance (EPR) has become an important spectroscopic tool in physics, chemistry, biology, and materials science to evaluate small hyperfine interactions and nuclear quadrupole couplings in solids, to study short-lived paramagnetic species, and to investigate the dynamics of paramagnetic compounds (*1–5*). In particular, one- and two-dimensional electron spin echo envelope modulation (ESEEM) techniques and pulse electron nuclear double resonance (ENDOR) methods have become very popular in the past couple of years.

The great majority of the pulse EPR spectrometers work at X-band frequencies (9 GHz). Recently, pulse EPR spectroscopy at microwave (mw) frequencies of about 95 GHz (W-band) and higher (*6–10*) as well as below 9 GHz (*11, 12*) have become of much interest. However, only a few pulse EPR spectrometers are capable of measuring electron spin echoes (and ESEEM) or free induction decays (FID) in the frequency range between X-band and W-band (*13–17*). This is in contrast to continuous wave (cw) EPR spectroscopy, where Q-band (35 GHz) frequencies are used routinely.

ENDOR and ESEEM experiments at Q-band frequencies have a number of advantages compared to the corresponding experiments at X-band and W-band. At 35 GHz the static magnetic field B_0 is often sufficiently high to separate EPR spectra of different paramagnetic species, resolve features belonging to different g principal values in disordered systems, and separate ENDOR (or ESEEM) lines of different nuclei. With increasing mw frequency, and correspondingly increasing magnetic field, the quality of an ENDOR spectrum is subject to two competing processes, namely the increase in spin polarization and the reduction of the hyperfine enhancement of the radiofrequency (RF) field (*18*). At Q-band frequencies spin polarization and the enhancement factor represent a good compromise for resolution and sensitivity.

Concerning the application of ESEEM spectroscopy, several situations must be distinguished. In the case of weak hyperfine couplings the ESEEM amplitude will decrease with increasing magnetic fields (*2*), so that ESEEM at Q-band is superior to W-band. In the case of strong hyperfine couplings, the modulation amplitude is often larger at higher mw frequencies due to a stronger state mixing. If the so-called cancellation condition is fulfilled, the modulation amplitude is maximum at a particular magnetic field and mw frequency (*19*). For such situations, Q-band frequencies represent their own niche to combine hyperfine couplings and nuclear Zeeman interactions.

The large bandwidth, the high quality factor, and the moderate filling factor make standard Q-band mw cavities convenient for pulse applications. In this frequency range mw components are still comparable in quality with X-band components, and the technical specifications make the construction of a pulse Q-band EPR spectrometer straightforward.

[1] On leave from MRS Laboratory, Kazan State University, Kazan, 420008, Tatarstan, Russian Federation.

1090-7807/01 $35.00
Copyright © 2001 by Academic Press
All rights of reproduction in any form reserved.

It has been demonstrated that pulse ENDOR and ESEEM experiments at Q-band frequencies can be carried out by using a slightly modified low-power superheterodyne EPR spectrometer (*13*). With this setup a number of standard pulse EPR experiments have been carried out on some particular samples. Better performance was obtained with an incoherent instrument using a pulsed IMPATT generator as the mw source (*14, 20*). Recently, a coherent high-power spectrometer has been described which uses homodyne detection and a TWT amplifier for the mw pulses (*15*). These authors also discussed sensitivity aspects of ESEEM and pulse ENDOR experiments at Q-band and presented a number of applications using standard pulse schemes.

So far, advanced pulse EPR methods have not been implemented at Q-band frequencies. One of these techniques is hyperfine sublevel correlation (HYSCORE) spectroscopy (*21*), which has become a standard tool for measuring small hyperfine couplings of paramagnetic species. Besides HYSCORE, a number of more sophisticated correlation experiments have been invented, for example, double nuclear coherence transfer (DONUT-HYSCORE) (*22*) and hyperfine correlated ENDOR (HYEND) experiments (*23*). For weak hyperfine couplings the potential of HYSCORE at Q-band is somewhat reduced because of the lower modulation depth compared with X-band. In such a situation, an improved coherence-transfer scheme based on matched mw pulses implemented early at X-band frequencies can be utilized (*24–26*).

In this work we describe a versatile high-power Q-band pulse EPR/ENDOR spectrometer. It is based on the design of pulse X- and S-band EPR spectrometers (*11, 27*) and recent developments in mw devices, acquisition electronics, and spectrometer software. The pulse spectrometer, which consists of four mw channels, two mw sources, and a pulse ENDOR accessory with two RF channels, has excellent performance for one- and two-dimensional routine measurements, as well as for the development of new pulse methodology. The experimental examples given in this work not only demonstrate the performance of the spectrometer but also illustrate that most of the modern pulse EPR methodology developed for X-band spectrometers can easily be implemented at Q-band.

SPECTROMETER DESCRIPTION

The spectrometer is designed as a multipurpose instrument for cw and pulse EPR and for pulse ENDOR experiments. A simplified block diagram of the mw part of the spectrometer is shown in Fig. 1. Isolators, direct current blocks, and frequency monitoring circuits are not shown. Series production and custom ordered mw components are implemented. The later ones are optimized according to the requirements of the pulse EPR experiments in the frequency range from 34.5 to 35.5 GHz. Commercial components will be characterized by company names, models, and specifications; custom-ordered components will be described by their parameters.

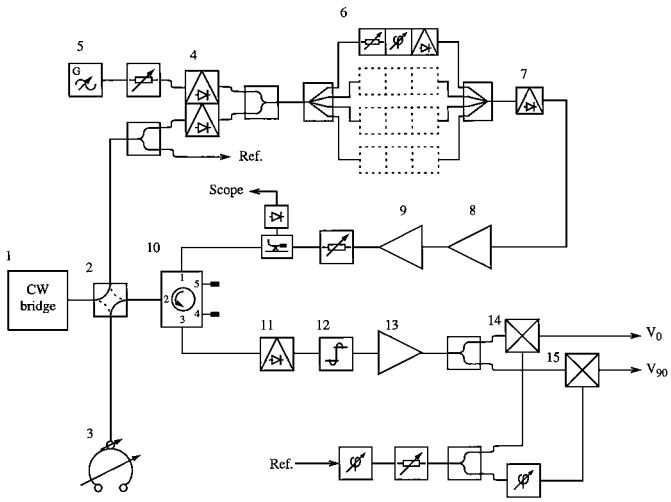

FIG. 1. Simplified block diagram of the Q-band mw bridge. The main components are as follows: (1) E-110 Varian bridge; (2) mechanical waveguide switch; (3) probe head; (4) electronically controlled commutator; (5) Gunn oscillator; (6) pulse forming unit; (7) fast mw switch; (8) solid state preamplifier; (9) travelling wave tube amplifier, TWT; (10) five-port circulator; (11) protecting switch; (12) limiter; (13) low noise mw preamplifier; (14, 15) orthomodal mixers. Microwave isolators and dc blocks (not shown) are used at critical points.

A Varian E-110 cw bridge (1) with a klystron (Varian, V1201) supplied by a console (Varian, E-Line E109) serves as the main mw source in the 34.5- to 35.5-GHz range. In the cw mode the bridge is connected to the probe head (3) via a motor-controlled waveguide switch (2) (Sector Microwave, VCFP). This mode allows one to measure cw EPR spectra as well as to adjust the frequency and coupling of the mw cavities. In the pulse mode, the mw power (50 mW) is directed from the bridge to the reference arm and the pulse-forming arm. Two diode switches form the mw source selector (4) and allow one to change the carrier frequencies during an mw pulse sequence. A second frequency source consists of a Gunn oscillator (5) (Spacek, GKa-50, 50 mW) with mechanical ($\pm$1 GHz) and voltage-controlled ($\pm$75 MHz) frequency tuning.

The pulse-forming block (6) has four channels; each of them is equipped with an absorption-type attenuator (0–30 dB), a phase shifter, and a fast mw switch with high-speed driver. High-quality movable waveguide shorts are used in the phase shifters to vary the mw phase in a stable way between 0 and 360°. An additional switch (7) is used to equalize the time parameters of the mw pulses in the different channels and further suppress the leaking mw power. All of the above-mentioned switches are distinguished by a short switching time (5 ns) and an isolation in the off state of 35 dB. The solid state amplifier (8) (MITEQ, AMF-5D, 26 dB) works as a preamplifier to drive the pulsed 100-W traveling wave tube (TWT) amplifier (9) (ASE, 187 Ka). The amplitude of the strongest mw pulse in a pulse sequence is typically tuned to a value such that the TWT operates just below the compression point. This allows for very stable high-power mw pulses with rise/fall times of 3 ns. To perform FT

EPR experiments where ultrashort mw pulses are required, the switch (7) is replaced by a fast switch with a rise and fall time of <1 ns (25 dB).

After passing the rotary attenuator (HP, R382A, 0–50 dB), the high-power pulses are fed to the input of the five-port circulator (10). A part of the mw power is directed to a diode detector to examine the pulses. The isolation of the circulator is improved by introducing a small dielectric disc into port 2 which acts as a tuning inhomogeneity. By an appropriate positioning of the disc, more than 42-dB attenuation of the wave propagating from port 1 to port 3 has been obtained within a 2-GHz range. This is at least 12 dB better than that obtained with a broadband factory tuning of this circulator.

All routine Q-band pulse EPR and ENDOR measurements are carried out with a commercial ENDOR probe head (Bruker, ER5106-QTE, 1.6 mm outer and 1 mm inner diameter sample tube, TE_{012} or TE_{013} mode, 35.2–35.5 GHz). With the slightly overcoupled cavity the two-pulse echo of γ-irradiated quartz is found to be maximum for mw $\pi/2$ and π pulses with lengths of 8 and 16 ns and an incident mw power of 100 W. The cavity ring-down time is less than 100 ns under these conditions. Homebuilt rectangular and cylindrical cavities for large sample tubes have been constructed and passed test measurements.

Signal detection is performed by a direct-gain receiver equipped with a quadrature detector. The low-noise amplifier (13) (noise figure is 4.3 dB) is protected against high-power pulses by the switch (11) (75 ns recovery time) and the limiter (12) (40 ns recovery time). The quadrature detector is based on orthomodal balanced mixers (14,15) (5.9-dB conversion losses). Rectangular waveguides (WR28) and coaxial cables (Huber + Suhner, Sucoflex 102) are used to connect the mw components. The quality of the connections was optimized using a vector network analyzer (Hewlett Packard, HP8722D).

In the pulse ENDOR mode, the RF is generated by an arbitrary waveform generator (LeCroy, LW420, 0–100 MHz). A homebuilt modulator is used to form the RF pulses. Two RF pulses which differ in frequency and phase can be produced. A distributed RF amplifier (Kalmus, 137C, 0.01–220 MHz) amplifies the RF pulses up to a level of 1 kW. With the Bruker probe head, RF pulses with a power of 200 W generate an RF field of $B_2 = 0.9$ mT (rotating frame) at the proton resonance frequency of about 55 MHz when the RF coil is terminated via a 50-Ω resistor. A calibrated current-to-voltage transformer is used to control the RF pulses. Rabi oscillations of weakly coupled protons were used to get reference values for B_2. The conversion factor of the ENDOR coil was found to be $\Lambda = \frac{B_2}{\sqrt{P}} \approx 0.06$ mT/$\sqrt{\text{W}}$.

The magnet (Bruker ER-073, 1.7 T, 56-mm air gap), the field controller (Bruker ER-032M), and the NMR gaussmeter (Bruker ER-035) allowed for an accurate setting and a precise control of the magnetic field. The mw frequency is measured with a frequency counter (XL Microwave, Model 3400). A continuous flow cryogenic system (Oxford Instruments (UK) Ltd., CF935) is used for all of the low-temperature measurements.

The spectrometer acquisition system is similar to the one reported earlier (*28*). It consists of a digital word generator (Interface Technology, RS690, 250 MHz), a gated integrator (SRS, SR250), a data acquisition board (Keithley, DAS1202), a GPIB interface, and a user-friendly acquisition program which runs on a personal computer. The instrument library of the program is extended by the arbitrary waveform generator (LeCroy, LW420), and the experiment library is expanded for experiments such as matched ESEEM, HYSCORE (*26*), PEANUT (*29*), and a number of other state-of-the-art sequences. The transient signals are recorded with a digital oscilloscope (LeCroy, LC534, 1-GHz analog bandwidth).

PERFORMANCE AND EXAMPLES

Davies ENDOR

First, we present a pulse ENDOR experiment on a copper-doped α-glycine single crystal. The hyperfine principal values 32.86, 20.66, and 17.4 MHz have been reported for the two directly coordinated and magnetically equivalent nitrogen ligands (*30*). The Davies ENDOR experiment performed at arbitrary crystal orientation shows two well-resolved doublets centered at 9.23 and 16.46 MHz with corresponding splittings of 0.6 and 0.2 MHz (Fig. 2). The spectrum was obtained with an RF pulse of length 30 μs and an RF power of 200 W.

Hyperfine Enhancement and Nuclear Nutation

The next example should give a feeling for the hyperfine enhancement of ENDOR experiments at Q-band by measuring the enhancement factor of the ^{14}N transition observed in Fig. 2.

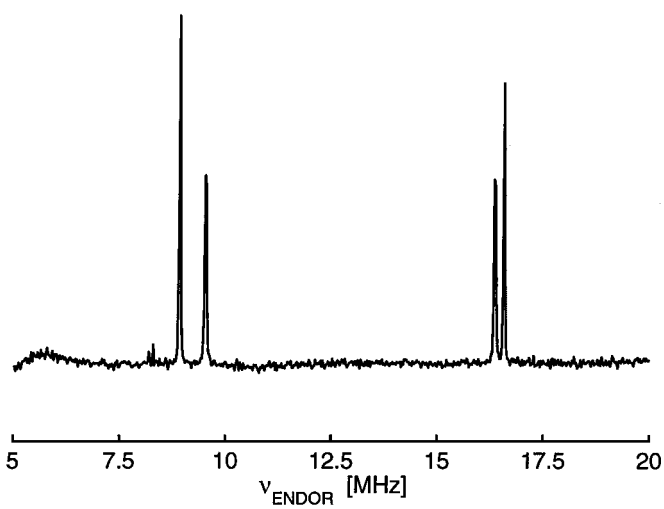

FIG. 2. Davies ENDOR spectrum of directly coordinated ^{14}N nuclei of Cu(II) (glycine)$_2$ in an α-glycine single crystal, recorded at $\nu_{mw} = 35.32$ GHz, $B_0 = 1.2068$ T, and a temperature of 25 K, with the pulse sequence π–t_{RF}–$\pi/2$–τ–π–τ–echo, with mw $\pi/2$ pulse of length $t_{\pi/2} = 40$ ns, a delay time $\tau = 200$ ns, and an RF pulse of length $t_{RF} = 30$ μs.

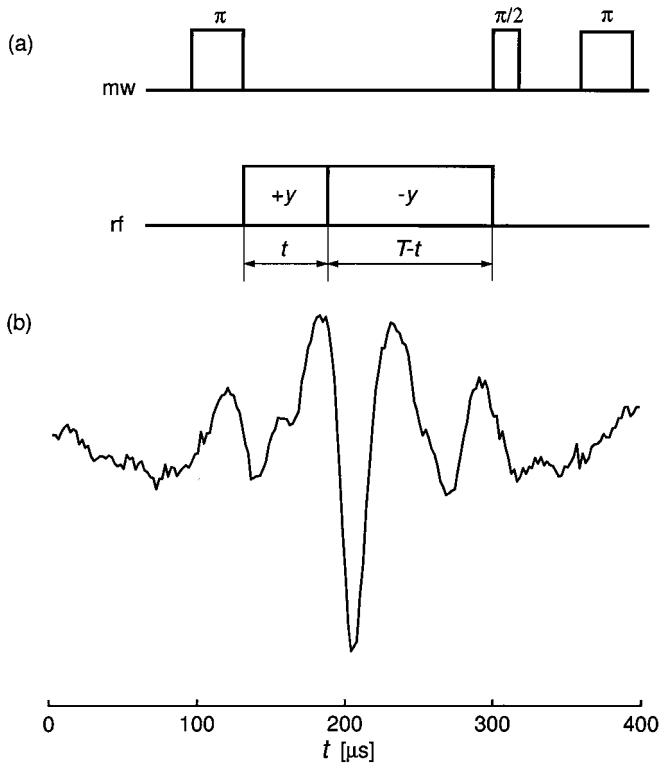

FIG. 3. Transient nutations of nitrogen nuclei resonating at 16.56 MHz (high-frequency line in Fig. 2). (a) Pulse sequence with two RF pulses of opposite phase. (b) Oscillations of the electron spin echo as a function of time t.

This is achieved by comparing the nutation frequency of the nuclei coupled to the unpaired electron with the corresponding frequencies in the absence of hyperfine coupling.

A new pulse sequence is introduced for the measurement of nutation frequencies of nuclei, which is based on a nuclear rotary echo experiment (*31*) and which uses an electron spin echo to record the nuclear transient nutation (Fig. 3a). The first selective mw π pulse creates two-spin order (*32*). The nuclear polarization evolves then under a composite RF pulse of constant length T, with a first pulse segment of variable length t with the B_2 field along the rotating frame $+y$ axis, followed by a second pulse segment of variable length $(T - t)$ with B_2 along the $-y$ axis. For $t = T/2$ a nuclear rotary echo is created. The nuclear transient polarization is indirectly measured via a two-pulse echo sequence by recording the polarization of the EPR transition, which has a level in common with the nuclear transition. For the measurement of nutation frequencies of nuclei with low gyromagnetic ratios, this approach is more convenient than monitoring the Rabi oscillations in a Mims or Davies ENDOR experiment. This is because in the rotary echo experiment the nuclear polarization oscillates at twice the nutation frequency and the B_2 inhomogeneity is partially refocused as in a PEANUT experiment (*29*).

The rotary echo experiment at the high-frequency line ($\nu_{\mathrm{RF}} =$ 16.56 MHz) of the ^{14}N ENDOR spectrum in Fig. 2 shows that for an RF power of 100 W the effective nitrogen nutation frequency is $\nu_{\mathrm{nut}} = 7.7$ kHz (Fig. 3b). Using the conversion factor of the RF coil $\Lambda \approx 0.06$ mT/$\sqrt{\mathrm{W}}$ known from proton ENDOR measurements and assuming that Λ at about 16 MHz and at the proton resonance frequency (54.4 MHz) are the same, a B_2 field of 0.6 mT is found at 16.56 MHz, resulting in an enhancement factor $\epsilon^{+}_{\mathrm{exp}} = \frac{\nu_{\mathrm{nut}} h}{g_{\mathrm{n}} \beta_{\mathrm{n}} B_0} \approx 4.1$, where g_{n} is the nuclear g value of the nitrogen nucleus. This enhancement factor is close to the theoretical value $\epsilon^{+}_{\mathrm{theor}} = 1 + \frac{Ah}{2 g_{\mathrm{n}} \beta_{\mathrm{n}} B_0} \approx 4.3$, where $A = \frac{(\nu_\alpha^2 - \nu_\beta^2) h}{2 g_{\mathrm{n}} \beta_{\mathrm{n}} B_0}$ is the hyperfine coupling and ν_α, ν_β are the observed ENDOR frequencies. For the low-frequency line of the ENDOR spectrum the factor is found to be $\epsilon^{-}_{\mathrm{exp}} = 2.4$, which is close to the value expected from $\epsilon^{-}_{\mathrm{theor}} = |1 - \frac{Ah}{2 g_{\mathrm{n}} \beta_{\mathrm{n}} B_0}| \approx 2.3$. The result indicates that for strongly coupled nuclei with a low magnetic moment like ^{14}N the ENDOR enhancement factor at Q-band is considerable, which still allows us to perform ENDOR experiments with relatively short RF pulses. For comparison, at 95 GHz the $\epsilon^{+}_{\mathrm{exp}}$ factor for the case at hand is about 2, and at 9.5 GHz it is approximately 13.

HYSCORE

The third example demonstrates that two-dimensional (2D) experiments can easily be implemented on the spectrometer. The HYSCORE experiment with the pulse sequence $\pi/2$–τ–$\pi/2$–t_1–π–t_2–$\pi/2$–τ–echo, was again performed on the copper-doped α-glycine single crystal with pulse length $t_{\pi/2} =$ 20 ns, $t_\pi = 16$ ns, and a time delay $\tau = 140$ ns. A total of 160 data points were taken in both time domains t_1 and t_2, with initial values of 40 ns. The dwell time was 24 ns, corresponding to a Nyquist frequency of 20.83 MHz. A four-step phase cycle was used (*33*). After baseline correction, apodization with a Gaussian window, and zero filling to 256 data points, the HYSCORE spectrum shown in Fig. 4 with an excellent signal-to-noise ratio was obtained. Two strong correlation peaks at (−16.44, 9.28) MHz

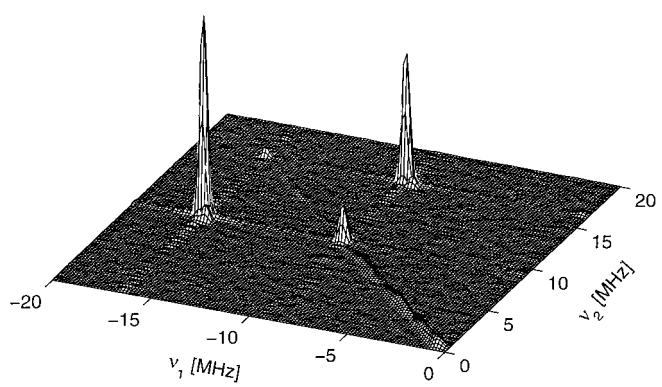

FIG. 4. Nitrogen HYSCORE spectrum of Cu(II) (glycine)$_2$ in an α-glycine single crystal (same orientation as in Fig. 2) recorded with the sequence $\pi/2$–τ–$\pi/2$–t_1–π–t_2–$\pi/2$–τ–echo, with mw pulses of length $t_{\pi/2} = 20$ ns and $t_\pi =$ 16 ns, a delay time $\tau = 140$ ns, initial values t_1 and t_2 of 40 ns, and a dwell time of 24 ns.

and (−9.28, 16.44) MHz are observed in the (−, +) quadrant, which are at least one order of magnitude more intense then the residual peaks on the main diagonal. The splittings observed in the ENDOR spectrum (Fig. 2) are not resolved in the HYSCORE experiment since we used a relatively poor resolution in the latter experiment because of measuring time limitation (3 h per 160 by 160 points).

Pulse Matching

The next example demonstrates the power of mw pulse matching at Q-band frequencies for enhancing the modulation depth. At X-band frequencies the three-pulse powder ESEEM experiment on vanadyl pyrophosphate hexadecahydrate, $VO(P_2O_7)_2$, diluted into the corresponding zinc compound shows proton and ^{31}P modulations (*34*), which disappear almost completely at Q-band frequencies. The decay of the stimulated echo measured with pulse length 12 ns ($\nu_1 \approx 21$ MHz) at a field position where all orientations contribute to the signal at Q-band is shown in Fig. 5a. From X-band and Q-band cw and pulse measurements, a predominantly isotropic ^{31}P hyperfine coupling of about 19 MHz is found. The Q-band HYSCORE spectrum of $VO(P_2O_7)_2$ shows correlation peaks which are slightly above the noise level (data not shown), whereas at X-band frequencies (ELEXSYS E580 spectrometer from Bruker) a signal-to-noise ratio of about 50 is found for the same number of accumulations (Fig. 6a). The observed correlations represented by ridges parallel to the main diagonal of the (−, +) quadrant have maxima at (−15.14, 3.42) MHz and (3.42, −15.14) MHz, resulting in an effective hyperfine coupling of 18.2 MHz.

Using matched three-pulse ESEEM (*26*), where the field strength (in frequency units) of the second and third mw pulses corresponds to the Zeeman frequency of the ^{31}P nuclei, $\nu_1 = \nu_I =$ 21 MHz results in a drastic increase in modulation depth when the length of the pulses is optimized. The time-domain trace recorded with the sequence $\pi/2$–τ–match–t–match–τ–echo, with $t_{\pi/2} = 12$ ns and $t_{\text{match}} = 60$ ns, is shown in Fig. 5b. In the corresponding spectrum a peak at the phosphorus Zeeman frequency and a doublet at 12 and 31 MHz are observed. The line

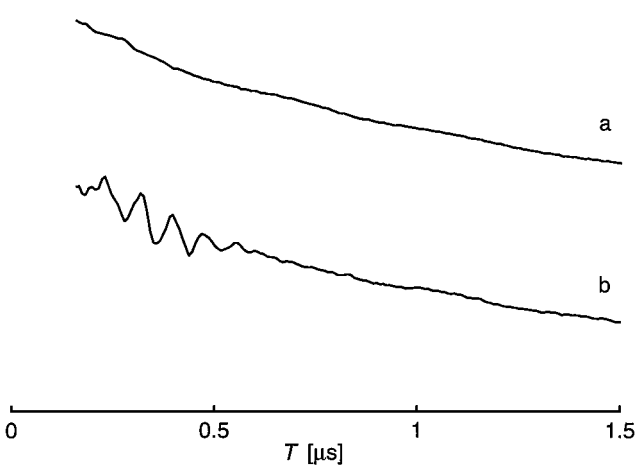

FIG. 5. Three-pulse ESEEM time traces of vanadyl pyrophosphate doped into a powder of zinc pyrophosphate hexadecahydrate, recorded at Q-band frequencies. (a) Conventional experiment with $\pi/2$ pulses of length $t_{\pi/2} = 12$ ns. (b) ESEEM with a matched second and third mw pulse of length 60 ns. In both cases an mw field strength of 21 MHz was used. The envelopes are normalized to their maximum values.

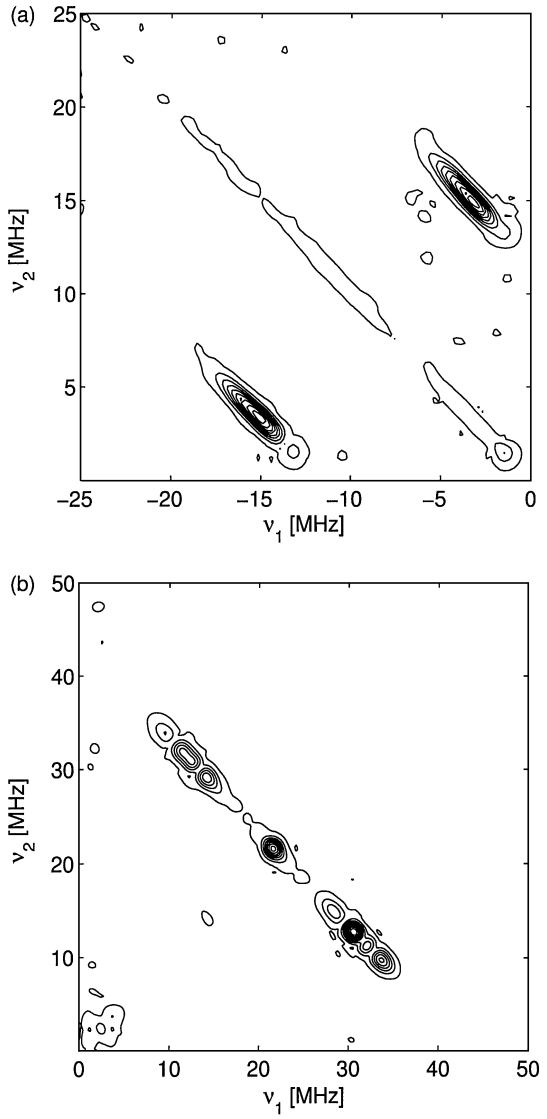

FIG. 6. X-band HYSCORE and matched Q-band HYSCORE spectra of vanadyl pyrophosphate doped into a powder of zinc pyrophosphate hexadecahydrate. (a) X-band spectrum recorded at $B_0 = 346.4$ mT and $\nu_{\text{mw}} = 9.7130$ GHz, with pulse lengths $t_{\pi/2} = 16$ ns and $t_\pi = 20$ ns, and $\tau = 132$ ns. A total of 256 data points are taken in both directions. (b) Q-band matched HYSCORE spectrum ($B_0 = 1.254$ T, $\nu_{\text{mw}} = 35.29$ GHz) obtained with the sequence $\pi/2$–τ–match–t_1–π–t_2–match–τ–echo, with $t_{\pi/2} = 12$ ns, $\tau = 148$ ns, $t_{\text{match}} = 60$ ns, $t_\pi = 24$ ns. A total of 128 × 128 data points are measured. The mw field is matched to the phosphorus Zeeman frequency of 21 MHz. A dwell time of 8 ns is used in both cases. Ten equidistant contours between 0.02 and 1 are shown, with contour level 1 corresponding to the maximum of the largest correlation peak. A polynomial baseline correction, apodization with a Gaussian window, and zero filling to 512 data points were used in both cases.

intensities show a periodic behavior as a function of the length of the matched pulses. The low-frequency line dominates the spectrum and is maximum for $t_{\text{match}} = 60$ ns, whereas the high-frequency line is very weak for $t_{\text{match}} < 45$ ns and again close to maximum for $t_{\text{match}} = 60$ ns.

The corresponding matched HYSCORE spectrum shown in Fig. 6b was performed with the sequence $\pi/2$–τ–match–t_1–π–t_2–match–τ–echo, with $t_{\pi/2} = 12$ ns, $\tau = 148$ ns, $t_{\text{match}} = 60$ ns, and $t_\pi = 24$ ns. The correlation ridges appear now in the (+, +) quadrant and are orthogonal to the main diagonal. The narrow peak on the diagonal at the phosphorus Zeeman frequency is caused by distant phosphorus nuclei.

In the X-band and the matched Q-band HYSCORE spectra shown in Fig. 6, the same data processing and the same contour levels (0.02–1) have been used. In both cases the peak amplitudes are normalized on their respective maxima. Figure 6 demonstrates that the signal-to-noise ratio in the matched Q-band HYSCORE spectrum is as good as the one in the standard HYSCORE at X-band. A hyperfine coupling of 18.0 MHz has been determined from the maxima of the correlation ridges in the Q-band spectrum. The slight difference in the X-band data may be caused by blind spots in the correlation ridges, which can be avoided by recording several spectra with different settings of the time interval τ.

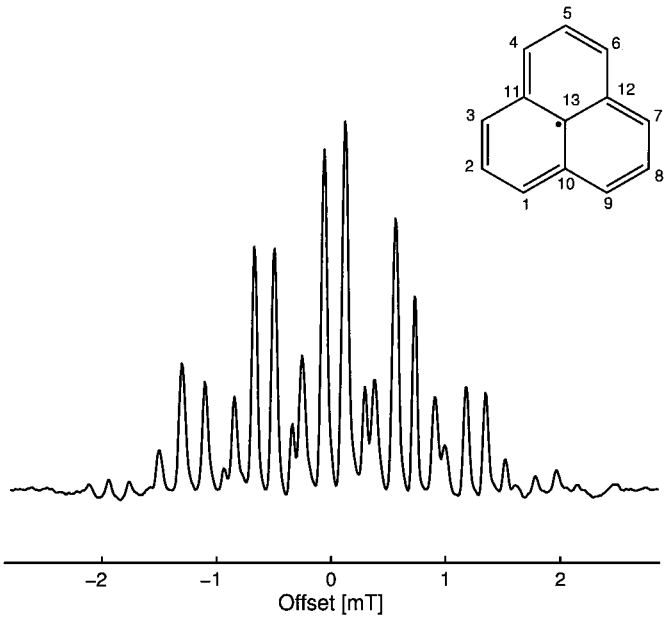

FIG. 7. Integrated Q-band cw EPR spectrum of the phenalenyl radical in solution at room temperature, recorded with an mw power of 0.5 mW, a modulation amplitude of 0.01 mT (100 kHz), a time constant of 0.25 s, and a sweep time of 10 min. The inset shows the structure of the phenalenyl radical. The six equivalent protons 1, 3, 4, 6, 7, and 9 have a hyperfine coupling of 17.61 MHz and the three equivalent protons 2,5, and 8 have a coupling of 5.05 MHz (*35*).

Fourier Transform EPR

The experimental examples given above illustrate some of the physical aspects of pulse EPR at Q-band. The next example demonstrates that the high mw power, the short mw pulse length, and the broad resonator bandwidth at this frequency band result in an excellent spectrometer performance for Fourier transform EPR experiments. The EPR spectrum of the phenalenyl radical spans a spectral width of about 4.3 mT (121 MHz). The hyperfine structure is due to two sets of equivalent protons (see inset in Fig. 7), three protons with a coupling of 5.05 MHz, and six protons with a coupling of 17.61 MHz (*35*). The integrated cw room temperature spectrum measured at 35.31 GHz in 10 min is shown in Fig. 7. An mw power of 0.5 mW and a modulation amplitude of 0.01 mT were used. The spectrum consists of seven quartets with intensities close to theoretical prediction 1 : 6 : 15 : 20 : 15 : 6 : 1. The linewidth of about 0.07 mT is due to the high radical concentration and the inhomogeneity of the static magnetic field of about 0.03 mT/cm perpendicular to this field. Because of the field inhomogeneity, only a small sample volume (7 mm in a quartz tube with 1.6-mm outer diameter) was used.

A rectangular cavity (dimensions $7 \times 3.5 \times 8.6$ mm) operating in the TE_{102} mode is used for FT-EPR experiments in solution. The cavity is connected to the waveguide through a fixed iris (2.8 × 1.5 mm). With this iris dimensions and a Teflon insert which supports the 1.6-mm sample tube in the cavity, a quality factor of about 150 is obtained at 35.3 GHz. With a DPPH test sample, we found that the amplitude of the free induction decay signal generated by an mw pulse with a length of 2 ns and an incident power of 100 W decreases by 3 dB when the resonance frequency ν_0 is shifted by about 90 MHz from the mw carrier frequency ν_{mw}. This corresponds to an effective bandwidth of the spectrometer in the FT-EPR mode of about 180 MHz. For the generation of mw pulses with a length of 2 ns, the mw switch (7) in Fig. 1 has been replaced by a faster switch with a subnanosecond switching time. The shape of the mw pulse after the TWT amplifier is shown in the inset in Fig. 8. Pulse rise and fall times of 0.6 ns were measured using an amplitude mw detector and an oscilloscope with 1-GHz bandwidth. The ringing observed after the pulse is caused by the video circuit.

Magnitude FT-EPR spectra of the phenalenyl radical measured at $\nu_0 - \nu_{\text{mw}} \approx 0$ and $\nu_0 - \nu_{\text{mw}} \approx 101$ MHz, where ν_0 is the resonance frequency at the center of the spectrum, are shown in Figs. 8a and 8b. The frequency of the cavity was kept constant during these measurements. The mw frequency was 20 MHz lower in (b) than in (a), to allow for a partial compensation of the lost in excitation/detection efficiency, when the center of the cavity response curve does not coincide with the center of the EPR line. In both cases quadrature detection was used. The FID can be observed for approximately 1.5 μs. The decays were recorded with a LeCroy oscilloscope with 2.5 GS/s sampling rate, and an average over 1000 traces was taken during 30 s. Data acquisition was started 100 ns after the mw pulse to avoid the accumulation of noise from the TWT. The FT-EPR spectra nicely reproduce the cw EPR spectrum of the phenalenyl radical, except for the lines of the outer quartets which are 60 times

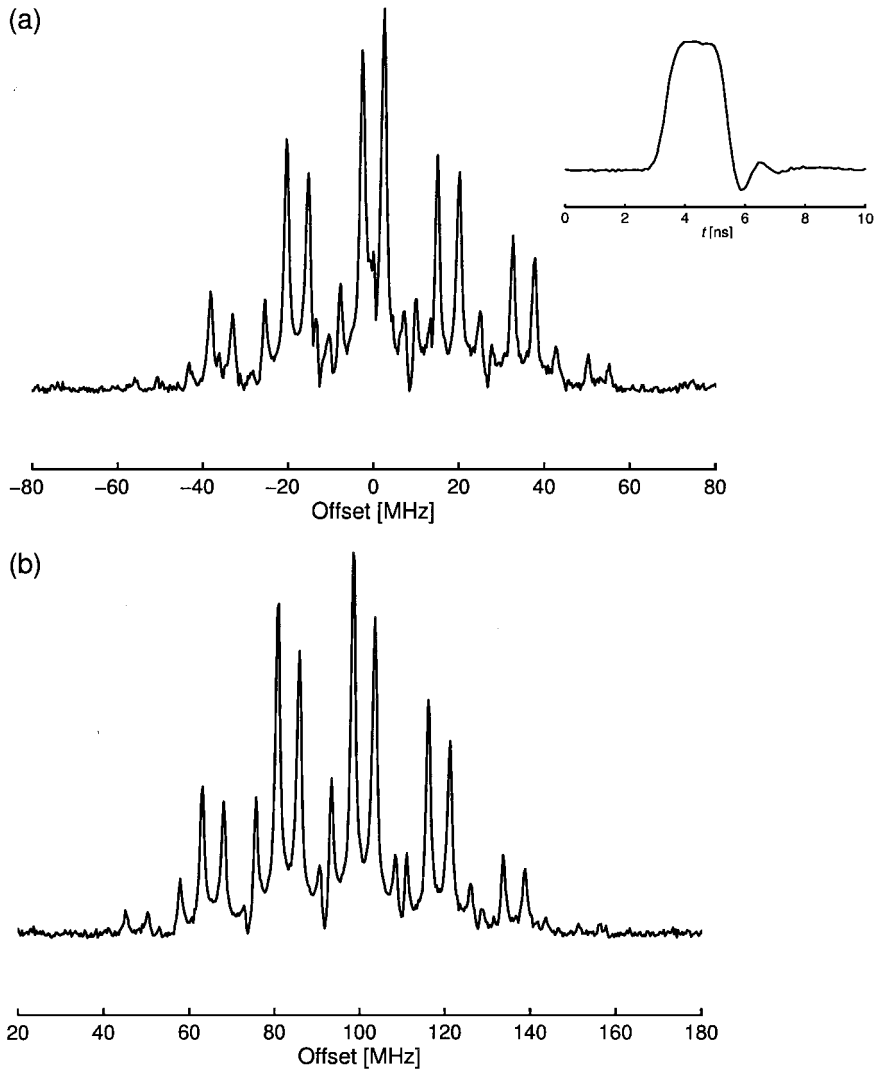

FIG. 8. Magnitude FT-EPR spectra of the phenalenyl radical at 35.3 GHz. (a) The carrier mw frequency coincides with the electron Zeeman frequency at the center of the spectrum. (b) Microwave and Zeeman frequencies differ by about 100 MHz. The spectra were recorded with an mw pulse of length 2 ns (shown in inset) and an incident power of 100 W. Quadrature detection was used. The average of 1000 FID signals digitized at 2.5 GS/s was taken. The repetition rate was 1 kHz and the measuring time was about 30 s. Apodization with a Gaussian window and zero filling were performed prior to Fourier transformation.

weaker than the strongest line in the spectrum. The FT-EPR spectra are slightly asymmetric because of a peculiarity in the shape of the cavity characteristic curve. Nevertheless, Fig. 8 demonstrates that it is possible to measure FT-EPR spectra at Q-band within a frequency band of about 120 MHz by using an overcoupled TE_{102} cavity and short pulses with 100-W incident mw power.

CONCLUSION

A high-power pulse EPR spectrometer operating at Q-band frequencies is described. The performance of the spectrometer is demonstrated by pulse ENDOR, conventional and matched HYSCORE, and FT-EPR experiments. The chosen experiments show, in addition to well-known features, performances which are specific for this frequency band. It is demonstrated that the classical rectangular Q-band resonator, operating in TE_{102} mode, provides a wide excitation bandwidth in FT-EPR experiments, that hyperfine enhancement allows one to perform pulse ENDOR of nuclei with low gyromagnetic ratios using relatively short RF pulses, and that even the loss in the modulation depth of ESEEM experiments can be compensated so that HYSCORE techniques can be used at Q-band widely. The examples illustrate that virtually all one- and two-dimensional pulse EPR experiments that require extended phase cycling procedures, two mw frequencies, or matching and decoupling pulses can be implemented at Q-band making use of all of the benefits of EPR at high frequencies. Recently, multiphoton echoes where an even

or an odd number of RF and mw photons is involved have also been studied with this spectrometer (*36*).

ACKNOWLEDGMENT

This research was supported by the Swiss National Science Foundation. We thank J. S. Hyde for the donation of a Q-band klystron. The assistance of K. Chernov and S. Orlinskii is gratefully acknowledged. We thank Hewlett Packard (Switzerland) for loaning out a network analyzer. We are grateful to Willi Groth for the mechanical construction of the bridge, the resonators, and the probe heads, to Lorenz Liesum for providing the X-band HYSCORE spectrum of vanadyl pyrophosphate, and to Walter Lämmler for sample preparation.

REFERENCES

1. A. Schweiger, Pulsed electron spin resonance spectroscopy: Basic principles, techniques, and examples of applications, *Angew. Chem. Int. Ed. Engl.* **30,** 265–292 (1991).

2. S. A. Dikanov and Yu. D. Tsvetkov, "Electron Spin Echo Envelope Modulation (ESEEM) Spectroscopy," CRC Press, Boca Raton, FL, 1992.

3. W. B. Mims, Electron spin echoes, *in* "Electron Paramagnetic Resonance" (S. Geschwind, Ed.), pp. 263–351, Plenum, New York, 1972.

4. L. Kevan and R. N. Schwartz (Eds.), "Time Domain Electron Spin Resonance," Wiley, New York, 1979.

5. L. Kevan and M. K. Bowman (Eds.), "Modern Pulsed and Continuous Wave Electron Spin Resonance," Wiley, New York, 1990.

6. T. F. Prisner, Pulsed high-frequency/high-field EPR, *Adv. Magn. Opt. Reson.* **20,** 245–298 (1997).

7. I. Gromov, V. Krymov, P. Manikandan, D. Arieli, and D. Goldfarb, A W-band pulsed ENDOR spectrometer: Setup and application to transition metal centers, *J. Magn. Reson.* **139,** 8–17 (1999).

8. P. Manikandan, R. Carmieli, T. Shane, A. J. Kalb (Gilboa), and D. Goldfarb, W-band ENDOR investigation of the manganese-binding site of concanavalin A: Determination of proton hyperfine couplings and their signs, *J. Am. Chem. Soc.* **122,** 3488–3494 (2000).

9. M. Bennati, C. T. Farrar, J. A. Bryant, S. J. Inati, V. Weis, G. J. Gerfen, P. Riggs-Gelasco, J. Stubbe, and R. G. Griffin, Pulsed electron-nuclear double resonance (ENDOR) at 140 GHz, *J. Magn. Reson.* **138,** 232–243 (1999).

10. M. T. Bennebroek and J. Schmidt, Pulsed ENDOR spectroscopy at large thermal spin polarizations and the absolute sign of the hyperfine interaction, *J. Magn. Reson.* **128,** 199–206 (1997).

11. M. Willer, J. Forrer, J. Keller, S. Van Doorslaer, A. Schweiger, R. Schuhmann, and T. Weiland, S-band (2–4 GHz) pulse electron paramagnetic resonance spectrometer: Construction, probe head design, and performance, *Rev. Sci. Instrum.* **71,** 2807–2817 (2000).

12. G. A. Rinard, R. W. Quine, R. Song, G. R. Eaton, and S. S. Eaton, Absolute EPR spin echo and noise intensities, *J. Magn. Reson.* **140,** 69–83 (1999).

13. R. de Beer, R. P. J. Merks, Observation of electron spin echoes at 35 GHz with a modified Ka-band EPR/ENDOR spectrometer, *Delft. Progr. Rep.* **4,** 63–66 (1979).

14. I. A. Gromov, S. B. Orlinskii, and R. M. Rakhmatoullin, Application of Q-band electron spin echo spectrometer to investigation of glasses doped with rare earth ions, *Appl. Magn. Reson.* **3,** 1147–1158 (1992).

15. C. E. Davoust, P. E. Doan, and B. M. Hoffman, Q-band pulsed electron spin-echo spectrometer and its application to ENDOR and ESEEM, *J. Magn. Reson. A* **119,** 38–44 (1996).

16. B. E. Sturgeon and R. D. Britt, Sensitive pulsed EPR spectrometer with an 8–18 GHz frequency range, *Rev. Sci. Instrum.* **63,** 2187–2192 (1992).

17. P. P. Borbat, R. H. Crepeau, and J. H. Freed, Multifrequency two-dimensional Fourier transform ESR: An X/Ku-band spectrometer, *J. Magn. Reson.* **127,** 155–167 (1997).

18. A. Abragam and B. Bleaney, "Electron Paramagnetic Resonance of Transition Ions," Clarendon Press, Oxford, 1970.

19. A. Lai, H. L. Flanagan, and D. J. Singel, Multifrequency electron spin echo envelope modulation in $S = 1/2$, $I = 1/2$ systems: Analysis of the spectral amplitudes, line shapes, and linewidths, *J. Chem. Phys.* **89,** 7161–7166 (1988).

20. I. A. Gromov, S. B. Orlinskii, and R. M. Rakhmatoullin, Rare earth ions environment in sodium borosilicate glasses studied with ESEEM spectroscopy, *Proc. XXVIII Congress AMPERE, Canterbury* 451–452 (1996).

21. P. Höfer, A. Grupp, H. Nebenführ, and M. Mehring, Hyperfine sublevel correlation (HYSCORE) spectroscopy: A 2D ESR investigation of the squaric acid radical, *Chem. Phys. Lett.* **132,** 279–282 (1986).

22. D. Goldfarb, V. Kofman, J. Libman, A. Shanzer, R. Rakhmatouline, S. Van Doorslaer, and A. Schweiger, Double nuclear coherence transfer (DONUT)-HYSCORE: A new tool for the assignment of nuclear frequencies in pulsed EPR experiments, *J. Am. Chem. Soc.* **120,** 7020–7029 (1998).

23. G. Jeschke and A. Schweiger, Hyperfine-correlated electron nuclear double resonance spectroscopy, *Chem. Phys. Lett.* **246,** 431–438 (1995).

24. G. Jeschke and A. Schweiger, Generation and transfer of coherence in electron-nuclear spin systems by non-ideal microwave pulses, *Mol. Phys.* **88,** 355–383 (1996).

25. G. Jeschke and A. Schweiger, Matched two-pulse electron spin echo envelope modulation spectroscopy, *J. Chem. Phys.* **105,** 2199–2211 (1996).

26. G. Jeschke, R. Rakhmatoullin, and A. Schweiger, Sensitivity enhancement by matched microwave pulses in one- and two-dimensional electron spin echo envelope modulation spectroscopy, *J. Magn. Reson.* **131,** 261–271 (1998).

27. Th. Wacker, Ph. D. Thesis, ETH, Zurich, No. 9913 (1992).

28. J. J. Shane, I. Gromov, S. Vega, and D. Goldfarb, A versatile pulsed X-band ENDOR spectrometer, *Rev. Sci. Instrum.* **98,** 3357–3364 (1998).

29. S. Stoll, G. Jeschke, M. Willer, and A. Schweiger, Nutation-Frequency correlated EPR spectroscopy: The PEANUT experiment, *J. Magn. Reson.* **130,** 86–96 (1998).

30. M. Fujimoto, C. A. McDowell, and T. Takui, Ligand ENDOR spectra of Cu(II) impurity complexes in α-glycine crystals, *J. Chem. Phys.* **70,** 3694–3701 (1979).

31. I. Solomon, Rotary spin echoes, *Phys. Rev. Lett.* **2,** 301–302 (1959).

32. R. R. Ernst, G. Bodenhausen, and A. Wokaun, "Principles of Nuclear Magnetic Resonance in One and Two Dimensions," Clarendon Press, Oxford, 1987.

33. C. Gemperle, G. Aebli, A. Schweiger, and R. R. Ernst, Phase cycling in pulse EPR, *J. Magn. Reson.* **88,** 241–256 (1990).

34. J.-M. Fauth, A. Schweiger, and R. R. Ernst, Recovery of broad hyperfine lines in electron spin-echo envelope modulation spectroscopy of disordered systems, *J. Magn. Reson.* **81,** 262–274 (1989).

35. F. Gerson, Notiz über das ESR.-Spektrum des Phenalenyl-Radikals, *Helv. Chim. Acta* **49,** 1463–1467 (1966).

36. I. Gromov and A. Schweiger, Multiphoton resonances in pulse EPR, *J. Magn. Reson.* **146,** 110–121 (2000).